Multi-scale Modelling for Studying Ductile Damage of Free Cutting Steel

Didier Farrugia, Boon Cheong

Swinden Technology Centre, Corus UK RD&T, Moorgate Rd, Rotherham, S603AR, UK

Abstract: This paper builds upon previous studies (Farrugia, 2006, 2008) for developing a more physical approach to predict the mechanisms of high temperature ductile damage acting at surface/sub-surface and across the length scale of continuously cast free cutting steel billet feedstock. A methodology combining mechanical testing and modelling has been developed to account for local microstructural heterogeneities such as MnS inclusions and used to refine the science of nucleation, growth and coalescence acting at high temperature for this range of low ductility steels. A 5-step modelling approach from macroscale damage criteria integrated into ABAQUS/Viewer to mesoscale elastoplastic and viscoplastic constitutive material models implemented as VUMAT into the ABAQUS/Explicit software (Lin et al, 2007) combined with microscale FEMs of inclusion behaviour has been developed to deal with aspect of physical length scale. To account for localization and bridging physical length scale, a two-scale transition Cellular Automaton Finite Element (CAFE) model (Shterenlikht, 2003) coupled with the meso-scale viscoplastic approach has also been implemented for refining prediction of damage in key representative volumes of mechanical test specimens. The multi-scale CAFE model is implemented into a VUMAT subroutine to compute the evolution of damage within each active cell within the CA array associated to each FE element. The CA has many advantages compared to other techniques as both physical and probabilistic/statistical knowledge can be implemented and tested via dissociation of material and FEM structure. Using this approach, a better characterisation of the underlying mechanisms of ductile damage can be achieved.

1. Background

The drive towards higher contribution free cutting steels (FCS) with improved machinability and consistency is leading to a requirement for improved understanding and control of as-rolled surface quality, most critically for steels which have a low ductility and narrow temperature range for defect free rolling. This is especially important during the transition from as-cast to wrought structure where the intrinsic reheated cast ductility can be as low as 10%. Physical understanding during rolling of the causes and mechanisms of damage initiation, growth and coalescence across the physical length scale at high temperature [850-1200^{o}C] and moderate strain rate [0.1-10s^{-1}] has not been up to now a major focus of interest (Figure 1), compared to developments in room temperature brittle and ductile fracture, and creep-superplasticity failure.

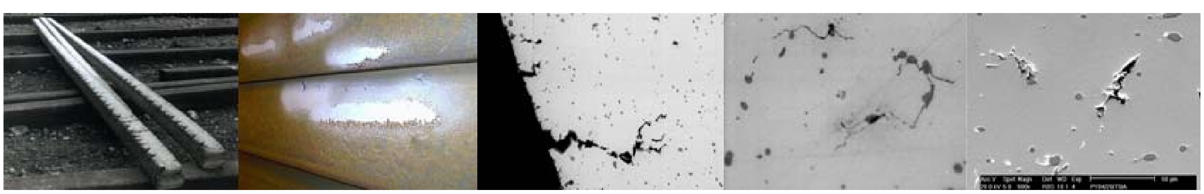

Figure 1. Damage in FCS steels and length scale effect (left to right: macro corner crack defects to micro-cracking around MnS inclusions).

The ductility is known to be dependent on geometrical and microstructural heterogeneities of the as-cast structure (chilled zone, casting surface/sub-surface defects, oscillation marks, second phase non-metallic inclusion (MnS distribution, morphology and spacing, etc.), the reheating practices and the influence of thermo-mechanical conditions during rolling (e.g. triaxiality inc. inversion, principal stress, strain, strain rate, heat losses, etc.). At mesoscale, interaction of triaxiality-equivalent strain is fundamental to nucleation and growth, mostly with presence of second phase particle (interface MnS/steel matrix influence). Coalescence is more of a function of principal stress direction and strain, exc. all microstructure effects (Farrugia 2008, Liu et al 2005, Lin et al 2007, Foster et al, 2005). Therefore cracking can proceed beyond triaxiality inversion and will be dependent solely on principal stress, dislocation density (strain), microstructural features (second phase inclusion, spacing, etc.) and intrinsic ductility of matrix. Triaxiality-strain at rupture changes according to

mechanical testing as per Rice & Tracey evolution with strain at rupture increasing as triaxiality reduces (Figure 5 (b)).
This paper builds upon previous studies by the same author (Farrugia, 2006, 2008) and describes the development and application of a modelling framework using the ABAQUS FEM software (6.6 to 6.8) for addressing the multiscale nature of high temperature ductile damage. This work, still in development, is part of a wider approach integrating advanced mechanical testing on a Gleeble thermo-mechanical simulator using a combined method of tensile and compression revised plane strain testing (RPS), laboratory rolling, detailed microstructural characterisation of nucleation, growth and coalescence amongst other activities.

The modelling framework based on ABAQUS/Explicit integrates a range of models and approaches from macroscopic-mesoscopic level to detailed microscopic and multiscale models based on Cellular Automata Finite Element approach. Table 1 summarises the approach which consists of:

1. Development and application of a range of a-dimensional mechanical parameters and simple damage criteria to provide a means of comparing mechanical testing (inc. design) with rolling conditions. Parameters listed in Section 2.1 such as triaxiality, principal stress and strain ratios have been formulated and computed. It should be noted that ABAQUS 6.8 now provides triaxiality plot directly (TRIAX variable). These parameters can be instantaneously predicted or integrated through the strain path or combined in typical plots of interest such as triaxiality-strain plot as per Rice and Tracey model (Rice and Tracey, 1969). In the absence of the possibility to automatically compute in ABAQUS well known damage criteria such as those of Cockcroft Latham (1966), Oyane (1972) and Lemaitre (1984), a C++ code has been developed to integrate state variables and compute efficiently in large meshes/models damage criteria such as the one from Lemaitre (shown in this paper).
2. Development and application of mesoscopic coupled constitutive damage models using the "simple" ductile damage model in ABAQUS/Explicit based on nucleation and evolution of damage.
3. Development and application of advanced phenomenological material models requiring VUMAT implementation and capable of describing within a viscoplastic formulation the evolution of various damage components such as induced by plasticity or grain boundary and metallurgical phenomena.
4. Microscale FEMs ranging from the elastoplastic or viscoplastic description of a representative volume element (RVE) consisting of austenite matrix and inclusions with the view to predict MnS inclusion behaviour under various conditions, to polycrystal plasticity models as developed by Dunne et al (2008). These models take into account inclusion spacing to diameter ratio, inclusion plasticity or crystallographic orientation and morphology to derive stress/strain partitioning effect which is present at the inclusion scale and explain the role of non-metallic inclusions in changing the strain distribution compared to the far field imposed strain on the austenite grain structure. More developments are required to account for cohesive strength, grain boundary interface modelling using approach such as cohesive zone modelling or XFEM.
5. Multiscale model based on CAFE approach as described in Section 4. A two-scale transition Cellular Automata Finite Element (CAFE) model (Shterenlikht, 2003) coupled with the meso-scale viscoplastic approach has also been implemented for refining prediction of damage in key representative volumes of mechanical test specimens (Farrugia, 2006). The multi-scale CAFE model is implemented into a VUMAT subroutine to compute the evolution of damage within each active cell within the CA array associated to each FE element.

Table 1: 5-step modelling approach for damage within ABAQUS

Type	Scale	Details
Criteria (time/strain integral of triaxiality/strain), e.g. Oyane, Lemaitre, Cocks, Cocroft, etc. + microstructure parameters (Field Variable)	Macro	Calibration/ Easy implementation $i_c \equiv \int_\Gamma \frac{p}{\sigma} d\bar{\varepsilon}$ $\begin{cases} D = 0 \text{ if } \varepsilon \leq \varepsilon_D \\ \dot{D} = \frac{D}{\varepsilon_R - \varepsilon_D}\left[\frac{2}{3}(1+\nu)+3(1-2\nu)\left(\frac{p}{\sigma}\right)^2\right]\dot{\varepsilon} \text{ if } \varepsilon > \varepsilon_D \end{cases}$
Simple Constitutive models	Meso	ABAQUS ductile damage model ABAQUS Gurson-Tvergaard
Phenomenological Constituitve Models (Birmingham, Imperial)	Meso + internal state	Normalised dislocation density, RX, GS, MnS spacing/diameter ratio
microFEMs of inclusion/matrix interaction to polyscrystal plasticity (Oxford) Global/submodelling	Micro	Global FEM/ Submodel Displacement 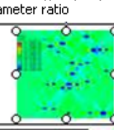
CAFE modelling (Sheffield, Corus)	Meso/Micro	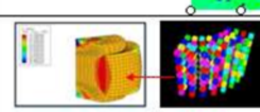

This knowledge has been put into practice with maximum effect in reducing surface defect rejection in production. Issues and future directions in terms of model development will be described in the rest of this paper.

2. Macro-mesoscopic ABAQUS FEM Models

2. 1 Key mechanical a-dimensional criteria for mechanical testing (and rolling)

Key normalised criteria (Farrugia, 2006) have been formulated and applied for a range of FEM ABAQUS mechanical tests and rolling simulations to quantify:

- the magnitude of the stress triaxiality ratio during testing

$$\mathrm{STR} = -\frac{1}{3} \cdot \frac{\sigma_{ii}}{\sigma_m} \tag{1}$$

A negative STR indicates a state of tensile triaxiality as σ_{ii} is equal to trace (σ_{ii}). σ_m is the equivalent stress. This can now be computed directly by including the variable TRIAX into the element output.

- the magnitude of the tensile principal stress ratio (>0) (σ_{III} is the longitudinal principal stress)

$$SPR = \frac{\sigma_{III}}{\sigma_m} \tag{2}$$

- The magnitude of the mid principal stress ratio (SMID)

$$\boldsymbol{SMID} = \frac{\boldsymbol{\sigma_{II}}}{\boldsymbol{\sigma_m}} \tag{3}$$

- The magnitude of average principal stress (according to McClintock, 1968)

$$\boldsymbol{SPRav = SPR + SMID > SPR} \tag{4}$$

- the magnitude of max-min principal strain ratio

$$\mathrm{PSR} = \frac{\varepsilon_{III}}{\varepsilon_I} \tag{5}$$

The lower and more negative this ratio is, the greater principal tensile strains are developed.

- the magnitude of the Mises - octahedral shear stress ratio

$$MOSSR = \frac{\sigma_m}{\frac{\sqrt{2}}{3} \cdot \sigma_{yy}} \tag{6}$$

- the magnitude of the max principal stress to the hydrostatic stress ratio

$$MHS = \frac{\sigma_{III}}{\sigma ii} \tag{7}$$

- Modified Argon (Argon, 2001)

$$Argon = \frac{PSR}{1 - STR} > 1 \tag{8}$$

Application of these criteria (triaxiality only) is shown in Figures 2 and 3, highlighting double collar, RPS and flying saucer type specimens the most suitable compression specimens for studying damage at high temperature for the range of triaxiality (> 0.33, < 0.8) required.

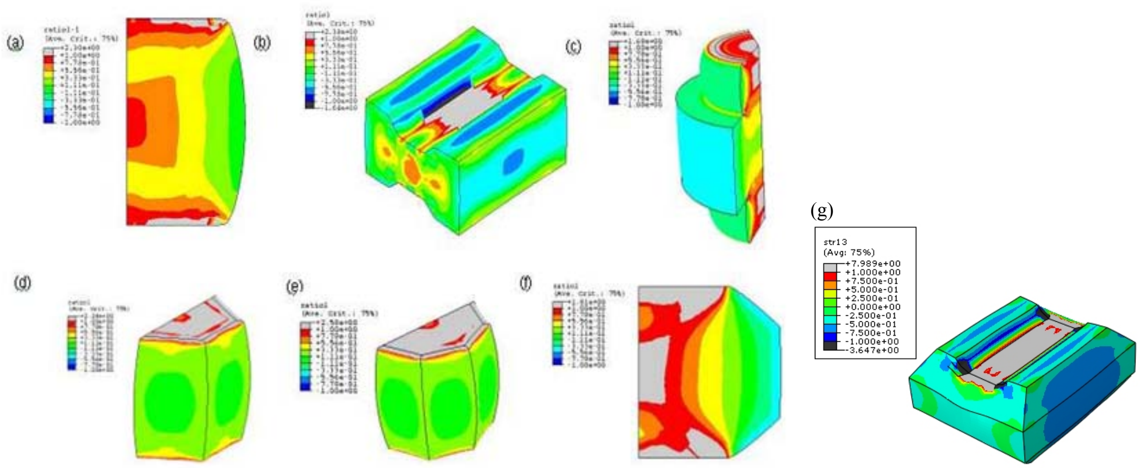

Figure 2. Triaxiality plot for a range of mechanical tests with high temperature damage (green to blue negative triaxiality, i.e. tensile at 33% reduction in height) (a) Upsetting (with friction) (b) Plane strain (c) Double collar (d) Hexagon compression (e) Octagon compression (f) Flying saucer / tapered billet (g) Revised plane strain (RPS) (Farrugia, 2006).

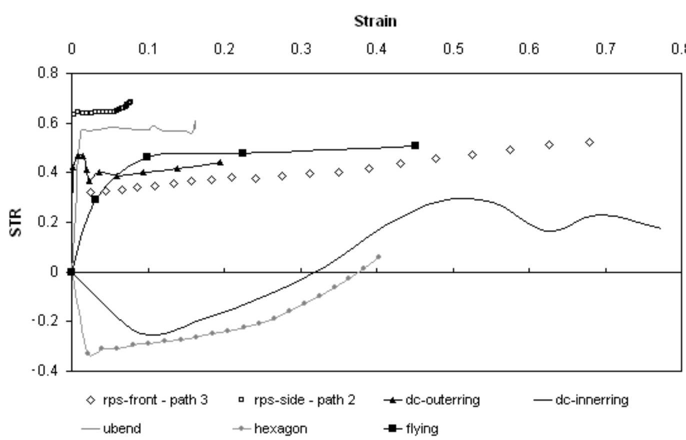

Figure 3. Triaxiality (STR) - strain plot for a range of mechanical tests (Farrugia, 2006).

This is to be compared with the stress states developed during rolling of blooms and billets during the transition of as-cast to a wrought structure as shown in Figures 4-5. Detailed analysis of the triaxiality and PSR ratios reveal that two regimes can be present in the roll bite, with or without inversion of triaxiality. This triaxiality inversion is in the longitudinal direction but a closer look (not shown) reveals that an inversion is also present through the stock thickness. Strain to failure-triaxiality curves obey a typical Rice and Tracey evolution (Figure 5 (b)). At triaxiality greater than 1 as demonstrated by Bandstra (2004), fracture strain is drastically reduced but independent of any further rise of triaxiality. The curve in Figure 5 (b) is useful in selecting mechanical testing. Torsion characterised by a zero or very low triaxiality can only generate local damage at medium to high strain (damage in shear). RPS and Plane Strain Compression (PSC) operates in the region of 0.2 to 0.9 STR, depending on curvature imposed (similar to rolling) and therefore cracking can be accelerated/reduced depending on conditions. Tensile testing after necking (at maximum load, triaxiality is 0.33), STR can rise to 2, therefore fracture will be rapid with minimum growth.

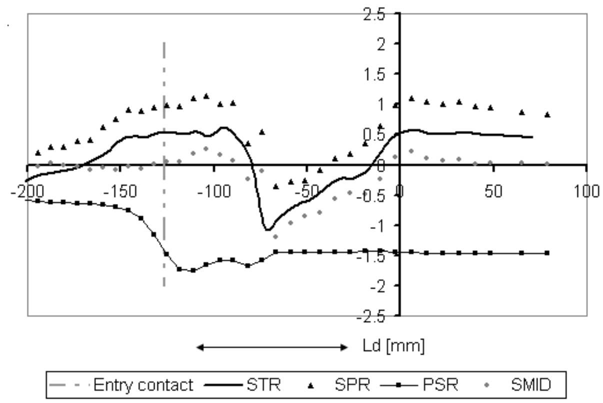

Figure 4. Typical longitudinal evolution of a-dimensional parameters (see definition above) at billet corner in the contact area during roughing passes.

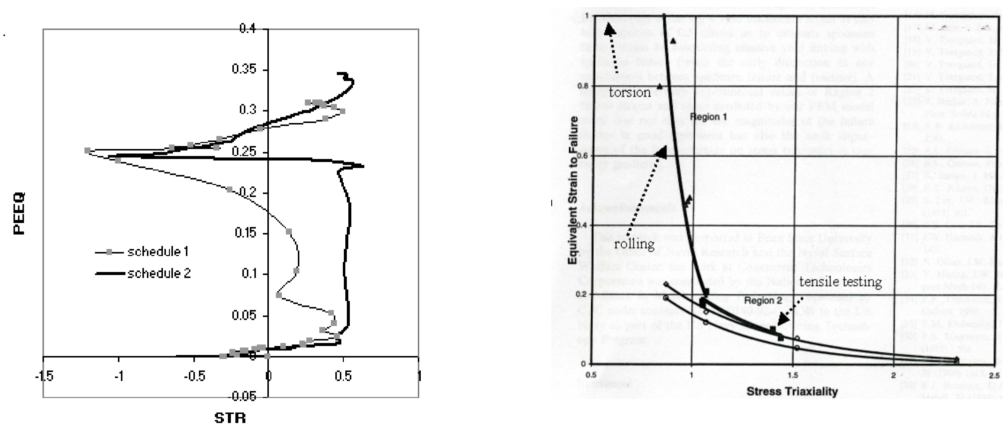

(a) **(b)**

Figure 5. (a) Typical triaxiality-strain (PEEQ) evolution at billet corner during box pass rolling for two rolling schedules (1 and 2) (b) Typical triaxiality (STR) - strain to failure (Bandstra, 2004).

2.2 Integrated ductile damage criteria with ABAQUS

Simple integrated ductile damage criteria have their benefits in highlighting zones where damage might be initiated but most of them are either empirical or macroscopic and do not differentiate on microstructural features (inclusions, DRX, grain size, etc.). They all tend to combine effect of either triaxiality or principal stress (growth/coalescence) with the accumulated strain to predict fracture. The constants appearing on the right hand side should be material dependent and calibrated by mechanical testing (mostly uniaxial tensile test). A good review in the literature is presented by Cescotto et al, 2002.

. **Cockcroft-Latham**

$$\int^{\bar{\varepsilon}_f} \frac{\sigma_{\max}}{\bar{\sigma}} d\bar{\varepsilon} = C_{CL} \tag{9}$$

This criterion is extensively used in the industry where values from 0.1 to 0.5 are usually predicted. This criterion does not take into account growth but is more targeted to coalescence. Zones at risk tend to be over-estimated and may not indicate the true location of initiation, for instance during tensile testing (Cescotto et al, 2002).

. **Lemaitre**

$$\begin{cases} \dot{D} = 0 \ \textit{if} \ \varepsilon \le \varepsilon_D \\ \dot{D} = \dfrac{D_c}{\varepsilon_D - \varepsilon_R}\left[\dfrac{2}{3}(1+\upsilon) + 3(1-2\upsilon)\left(\dfrac{p}{\bar{\sigma}}\right)^2\right]\dot{\bar{\varepsilon}} \end{cases} \quad \textit{if} \ \varepsilon > \varepsilon_D \tag{10}$$

D_c : Criterion at rupture, ε_D : Strain necessary to nucleate cracks in a uniaxial tensile test

ε_R : Strain at rupture determined for a uniaxial test. υ : Poisson coefficient (0.33)

p: hydrostatic pressure, $\bar{\sigma}$: equivalent stress, $\dot{\bar{\varepsilon}}$: equivalent strain rate

This criterion is well accepted in the ductile damage community. A high-performance postprocessor has been developed with the use of the ABAQUS C++ Application Programming Interface (API) to allow for the visualisation material information that is not readily available in the standard ABAQUS field output, material information such as this criterion. The postprocessor is compiled and linked using the ABAQUS make utility (*ABAQUS make job= postprocessor* command) and run using the ABAQUS execution procedure (*ABAQUS postprocessor sourceodb targetodb)* where sourceodb is the filename of the source output database and targetodb the target output database. Given the name of a source output database, from which the model, results, and standard field output information is to be read, the postprocessor produces a target output database, to which a selected part of the source model, results, and standard field output information will be replicated together with the addition of user-defined field output. Currently, the user-defined field output based on the Lemaitre damage formulation has been implemented. Formulations other than Lemaitre damage can be implemented in the future.

To select the part of the source model, results, and standard field output information that are to be replicated in the target output database, the postprocessor looks into the source output database for a given element set. This element set can be one that is defined in the **root** assembly or in a particular **part** instance. Elements that are associated with this element set will be replicated in the target output database by creating a new part, adding nodes using the same nodal coordinates and nodal numbering, creating the elements with same connectivity and finally instantiating the newly created part.

The postprocessor then looks into the result information in the source output database, by going incrementally through all the output frames. Each output frame in the source output database is replicated in the target output database. A selected set of standard field output information carried by each output frame is also replicated. This set of standard field output information includes the following field output variables:

- "U": This contains all physical displacement components, including rotations at nodes with rotational degrees of freedom. This field output variable is required for the visualisation of deformation.

- "S": This contains all stress components. This field output variable is required for the computation of Lemaitre damage.

- "PEEQ": This contains the equivalent plastic strain. This field output variable is required for the computation of Lemaitre damage.

In addition, the postprocessor computes and stores the following user-defined field output variables in the target output database:

- "d_PEEQ_dt": This contains the equivalent plastic strain rate. This field output variable is required for the computation of Lemaitre damage.

- "d_Lemaitre_dt": This contains the rate of Lemaitre damage. This field output variable is required for the computation of Lemaitre damage.

- "Lemaitre": This contains the Lemaitre damage.

As an example, Figure 6 (a) shows the field output of a target output database produced by the C++ postprocessor. Figure 6 (b) shows the computed Lemaitre damage variable contour plot. All facilities available in ABAQUS Viewer can be used within the target odb file such as history plot.

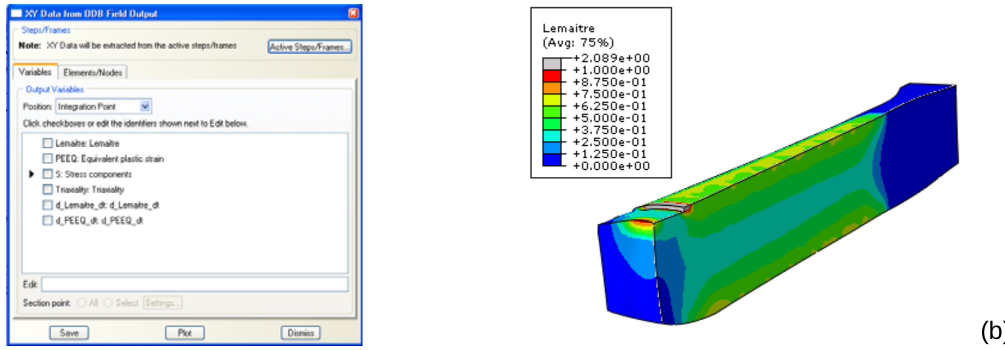

Figure 6. (a) Example field output of a target output database produced by the C++ postprocessor (b) Lemaitre damage output in rolled billet with front end crop (mid plane).

2.3 Mesoscopic coupled ductile damage (nucleation and coalescence)

The damage evolution "standard" capability in ABAQUS (i.e. without the use of a user material subroutine) has been used and calibrated. It is based on a damage initiation or nucleation and evolution criteria which are fully coupled in the sense that progressive degradation of the material stiffness leading to failure is modeled (see Figure 9 (a). The model uses mesh-independent measures either via plastic displacement (instead of strain) or energy dissipation. The RPS mechanical test (Figure 2 (g)) has been used to generate nucleation curves at different temperature and strain rate for a range of low carbon FCS steels for both monotonic and multi-hit tests (Farrugia, 2008). By machining RPS specimens with inclined front and backend faces together with side faces, one can generate in a single test, for a given reduction, temperature and strain rate regime, at least two states of stress-strain conditions, i.e. mid triaxiality and strain together with high triaxiality-low strain regions as per Figures 5 (b) and 9 (d). Detailed characterisation at both meso and microscale show that the RPS test is sensitive to the steel grade considered, microstructure orientation and thermo-mechanical conditions, the mid front horizontal plane (see path 3) being the likely plane for cracking as shown in Figure 7 (a). During RPS, all the various regimes from nucleation to coalescence for intergranular cracking, together with grain boundary cracking can be present. An incremental picture of damage evolution (from nucleation to coalescence) is shown in Figure 7 (b). The influence of MnS inclusions as studied by Paliwoda (1963) who proposed a critical ratio s/d < 2.7 (s: spacing, d: inclusion diameter) is shown in Figure 7 (c). Coarser inclusions closer to the surface, with reduced interspacing can act as stress/strain raiser.

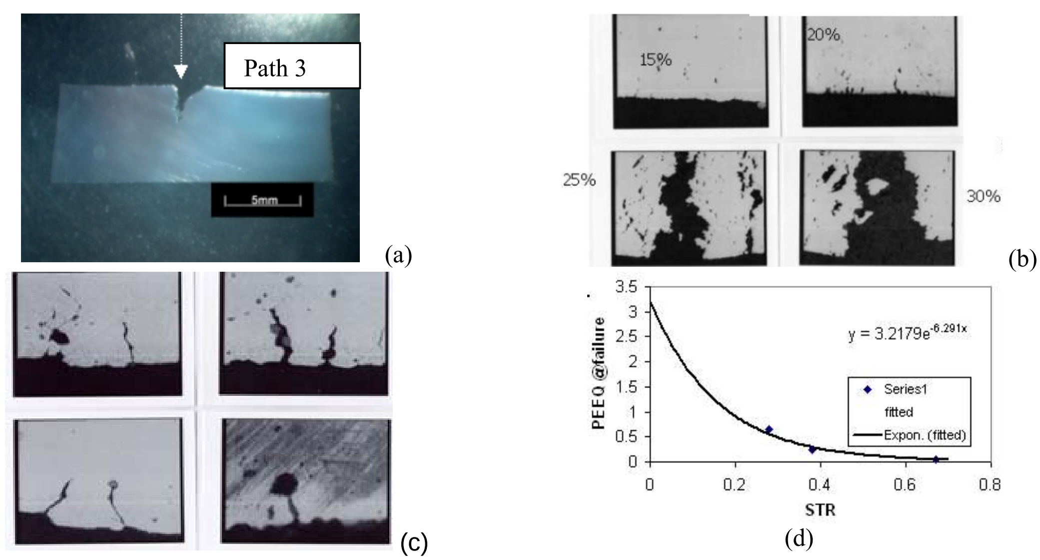

Figure 7. (a) Mid horizontal plane (half specimen) with arrow showing external surface. Cracking in direction to path 3 (outer mid plane to inner sample) (b) evolution during RPS testing of ductile damage (mid horizontal plane, path3) 880°C - 1s^{-1} (c) Influence of MnS inclusion spacing and diameter ratio closed to steel surface (path 3) (d) Example of nucleation curve input to damage model 1s^{-1} - 880°C.

The ABAQUS ductile model can be used with an element deletion feature to remove elements from the mesh (see card Figure 8 (a). It is accepted that accuracy, mostly with single integration point element (C3D8R or RT) will increase as mesh density increases in the area of damage nucleation/growth despite the fact that mesh independent criterion is used based on characteristic length of element. Section control for the element kinematic as well as key output variables can be incorporated as shown in Figure 8 (a) & (b).

```
** ELEMENT CONTROLS
** max degradation=0.99
*Section Controls, name=EC-1, hourglass=STIFFNESS, element deletion=yes, MAX DEGRADATION=0.95
1., 1., 1.
*Section Controls, name=EC-2, hourglass=STIFFNESS, element deletion=no
1., 1., 1.
**
```

(a)

```
*Element Output, directions=YES
EVOL, LE, PEEQ, S, TEMP,SDEG, DMICRT, STATUS
```

(b)

Figure 8. (a) Section controls for C3D8RT with element deletion in critical area (b) Typical element output for including stiffness degradation and nucleation critical ratio.

Figure 9 (a-d) illustrates the basic concept with the tabular damage evolution (displacement) selected in this case.

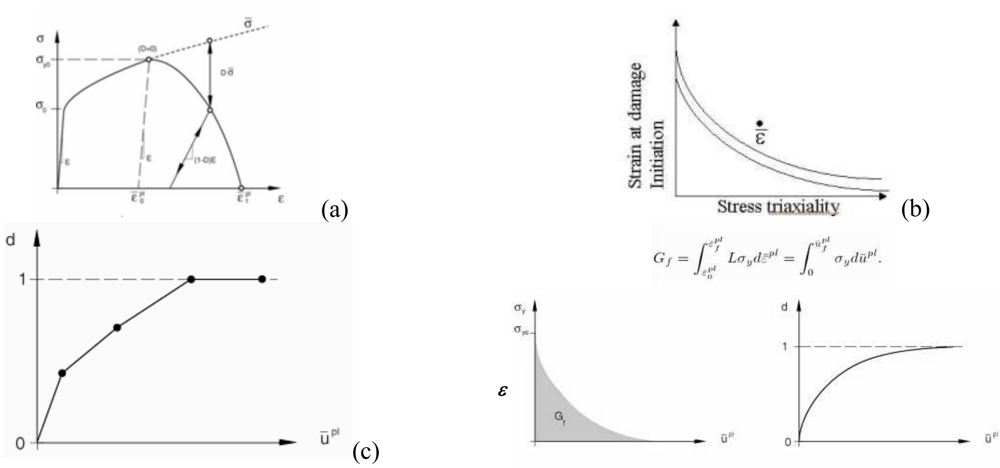

Figure 9 (a-d). ABAQUS Damage model principles (a) stress/strain to failure, (b) nucleation (c) tabular data input for damage evolution (d) fracture energy criterion (Hillerborg, 1976).

- **Damage nucleation (RPS compression testing)**

Nucleation curves have been constructed based on assessment of deformation and cracking for a range of FCS steels, see Figure 7 (d) and input as tabular data into the ABAQUS input deck. Use of the two plane of deformation has been made to extract value of equivalent strain and triaxiality. These cover the range of strain and triaxiality encountered during rolling. In order to develop the full curve, ideally an extra point is required. This can be obtained from a uniaxial compression test at high friction, giving higher strain and reduced triaxiality.

The fit is based on the Rice and Tracey model (fig.10) where $\varepsilon = \boldsymbol{A}.\exp(-\boldsymbol{B}.\frac{\sigma_m}{\overline{\sigma}})$ (11)

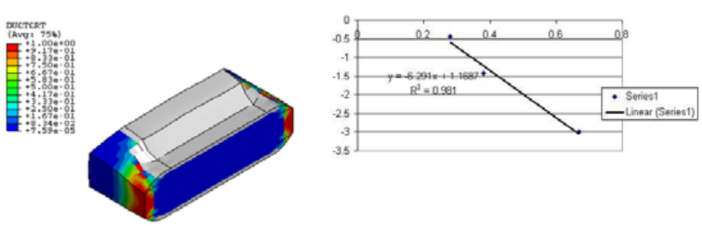

(a) (b)

*DAMAGE INITIATION, CRITERION=DUCTILE, DEPENDENCIES=*n*

1. Equivalent fracture strain at damage initiation
2. Stress triaxiality, $(-p/q)$.
3. Strain rate.
4. Temperature, if temperature dependent.
5. First field variable. ← e.g. Inclusion spacing/d ratio
6. Second field variable.
7. Etc., up to four field variables.

(c)

Figure 10. (a) ABAQUS RPS damage nucleation model (DUCTCRT) (b) Rice and Tracey nucleation fit, (c) typical ABAQUS Card.

- **Damage evolution (tensile testing)**

Stress strain data from tensile testing (Foster et al, 2008) have been used from the point of maximum loading (at start of necking, triaxiality STR =0.33) to develop stress and relative displacement data calculated from diameter at point of necking to final diameter at fracture (Figure 11 (a)). Integration of Figure 11 (a) leads to the definition of Energy concept Gf according to Hillerborg (1976).

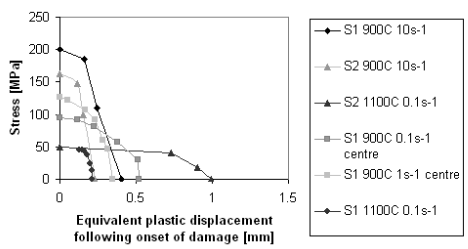

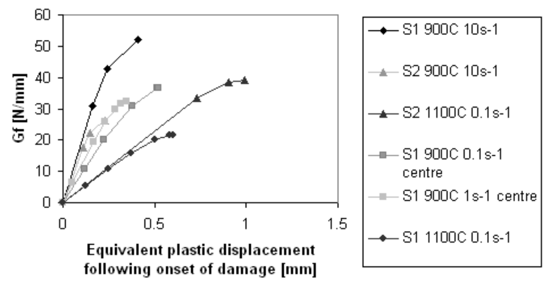

(a) (b)

Figure 11. (a) Stress-displacement (mm) curve used for damage evolution (b) Fracture energy Gf function of displacement (N/mm) , temperature and strain rate for two FCS steels

The model was applied to RPS specimen (Figure 12) with element deletion using criteria shown in Figures 11 (a) and (b).

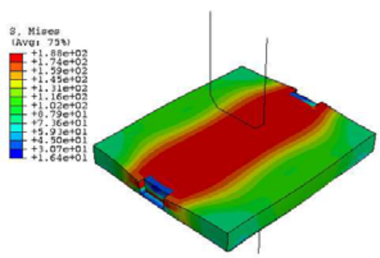

(a)

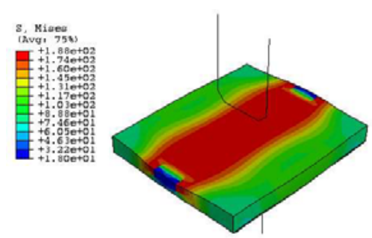

(b)

Figure 12 (a-b). FEM MISES damage evolution (a) with element removal (failure) due to damage evolution (displacement) (b) and energy based criterion (mid cut plane).

Application of submodelling is also of interest for damage modelling by mapping displacements to a submodel where finer discretisation can be used. In principle this concept could be applied several times to reach range of length scale of interest and provide a means of linking mesoscopic simulation with microFEMs as shown in Section 4. Figure 13 shows an example of application of submodelling within ABAQUS to the RPS test. Final discretisation reaches 25microns. Care is to be taken with respect to boundaries and mass scaling as mesh is refined.

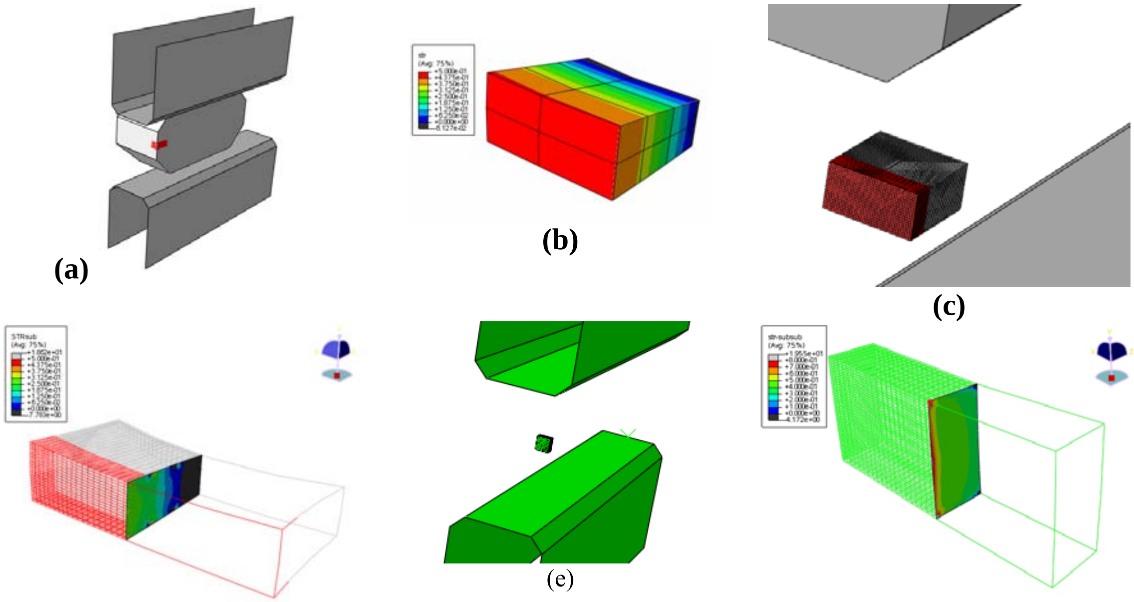

(a) (b) (c)

(d) (e) (f)

Figure 13. Application of sub-modelling through the length scale (a) Global RPS model with partition for submodelling - 500 microns discretisation (b) triaxiality contour plot in global mesoscopic partition (c) first length scale submodel (50 microns discretisation) (d) triaxiality plot in submodel (e) sub-sub model (surface effect) discretisation 25 microns (f) triaxiality plot in sub-submodel.

Damage nucleation and evolution can of course be applied to the submodel (Figure.14)

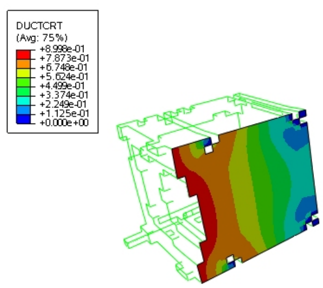

Figure 14. Ductile criteria threshold in submodel (mid plane of partition).

3. Phenomenological viscoplastic damage model

3.1 Viscoplastic damage model 1 (Liu et al, 2005)

A two-parameter viscoplastic constitutive model has been developed by Liu et al (2005) in collaboration with Corus. This model includes two types of damage parameters, which are strongly dependent on strain rate. Strain (through a normalised dislocation density approach), strain rate, recrystallisation, dynamic recovery, and grain size are taken into account in this approach. The equation set is shown in Figure 15. This model was fitted on FCS steels tensile data as presented in Figure 11 (a). At low strain rates, damage at grain boundary is dominant, whilst at higher strain rate (>0.1 s^{-1}), deformation by dislocation slip occurs and plasticity induced damage becomes dominant. Both damage parameters need to be integrated and the exponential rate of damage growth reduces the chance of both damage factors contributing evenly to failure. Damage evolution equations are based on nucleation and growth. By mapping damage nucleation to the rate of change of dislocation, damage healing can be taken into account. It should be noted that current implementation of damage in this model is not stress dependent; this has been addressed in Model 2. Figure 16 shows plasticity damage plots for the double collar test for a range of temperature conditions (1000°C (a), 727°C (b) and 1200°C (c)) and initial grain sizes (35 and 90 microns (d) at 1000°C).

$$\dot{\varepsilon}_p = A_1 \cdot \sinh\left[A_2 \cdot \left(\frac{\sigma}{1-D_{GB}} - (R+k)\cdot(1-D_{Pi})\right)\right] \Big/ \left(\frac{d}{d_0}\right)^{\gamma_1} \quad (1)$$

$$\dot{S} = H_1 \cdot (x \cdot \bar{\rho} - \bar{\rho}_c \cdot (1-S)) \cdot (1-S)^{\lambda_1} \quad (2)$$

$$\dot{x} = X_1 \cdot (1-x) \cdot \bar{\rho} \quad (3)$$

$$\dot{\bar{\rho}} = \left(\frac{d}{d_0}\right)^{\delta_1} \cdot (1-\bar{\rho}) \cdot \left|\dot{\varepsilon}_p\right|^{\delta_2} - C_r \cdot \bar{\rho}^{\delta_3} - \frac{C_S \cdot \bar{\rho}}{1-S}\dot{S} \quad (4)$$

$$\dot{R} = 0.5 \cdot B \cdot \bar{\rho}^{-1/2} \cdot \dot{\bar{\rho}} \quad (5)$$

$$\dot{d} = \left(\frac{G_1}{d}\right)^{\psi_1} - G_2 \cdot \dot{S} \cdot \left(\frac{d}{d_0}\right)^{\psi_2} \quad (6)$$

$$\sigma = E \cdot (\varepsilon_T - \varepsilon_p) \quad (7)$$

$$\dot{D}_{GB} = \eta \cdot \left(\left[a_4 \cdot (1-D_{GB}) \cdot \dot{\bar{\rho}}\right] + \left[\left(\frac{1}{(1-D_{GB})^{n_3}} - (1-D_{GB})\right) \cdot \left|\dot{\varepsilon}_p\right|\right]\right) \quad (8)$$

$$\dot{D}_{Pi} = a_5 \cdot \left(\left[(1-D_{Pi}) \cdot \dot{\bar{\rho}}\right] + \left[a_6 \cdot \frac{D_{Pi} \cdot d}{(1-D_{Pi})^{n_1}} \cdot \left|\dot{\varepsilon}_p\right|^{n_4}\right]\right) \quad (9)$$

$$\dot{D}_T = \dot{D}_{GB} + \dot{D}_{Pi} \quad (10)$$

where

$$\eta = a_1 \cdot \exp\left(-a_2 \cdot \left(1 - \frac{d}{d_c}\right)^2\right) \quad (11)$$

$$d_c = a_3 \cdot (\dot{\varepsilon}_p)^{-n_1} \quad (12)$$

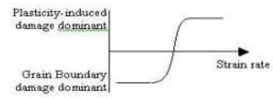

where ε_p is the plastic strain, ε_T the total strain, R the isotropic hardening, k the initial yield stress, d the average grain size, S the fraction of recrystallisation, x the parameter controlling the onset of recrystallisation, $\bar{\rho}$ the normalised dislocation density, D_{GB} the grain-boundary damage, D_{Pi} the plasticity-induced damage, D_T the total damage, E the Young's modulus, and σ the flow stress.

Figure 15. Constitutive viscoplastic model 1 (Liu et al, 2005).

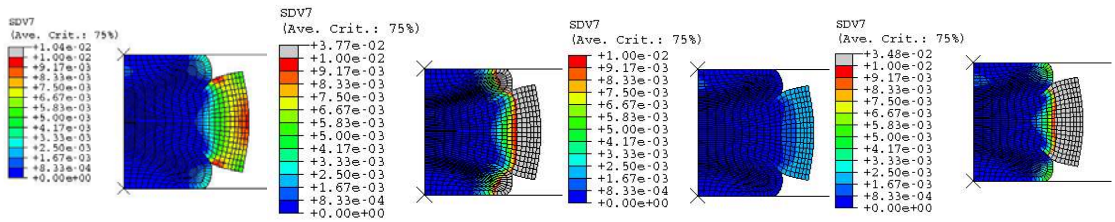

Figure 16. Plasticity damage plots (a) 1000°C, 35 microns, (b) 727°C, 35 microns, (c), 1200°C, 35 microns, (d) 1000°C, 90 microns.

3.2 Viscoplastic damage model Model 2 (Foster et al, 2008)

A revised and somehow simplified viscoplastic model has been developed to consider damage developed at inclusion and coalescence of microcrack to macrocrack due to void inclusion interaction and principal stress. The basic of the model and evolution equations which have to be integrated within a VUMAT ABAQUS framework are shown in Figure 17. The new enhanced model has been applied to the RPS mechanical test (Figure 18) taking into account a given spacing to diameter ratio of MnS inclusions. Nucleation is not modelled only assuming that a given threshold strain has to be reached before growth can occur (this simulates LFCS with weak cohesive strength). Growth at inclusion (Di) is then dependent on dislocation density (strain), triaxiality based on a Cocks and Ashby model (1982) and interspacing- size ratio of MnS inclusions. Coalescence (Dc) is dependent on principal stress, dislocation density and MnS spacing ratio.

$$\dot{\varepsilon}_p = \left\langle \frac{\frac{\sigma_e}{1-D_C} - (k+R)}{K} \right\rangle_+^n \qquad R = B\sqrt{\bar{\rho}}$$

$$\dot{\bar{\rho}} = k_1 \cdot \left(1 - \sqrt{\bar{\rho}}\right) \cdot \dot{\varepsilon}_p - c_1 \bar{\rho}^{c_2}$$

$$\dot{D}_i = z_1 \varpi \dot{\varepsilon}_p^{\gamma} \cdot \frac{\sinh\left(2\frac{(n_d - 1/2)}{(n_d + 1/2)}\frac{\sigma_H}{\sigma_e}\right)}{\sinh\left(\frac{2}{3}\frac{(n_d - 1/2)}{(n_d + 1/2)}\right)}$$

$$\dot{D}_C = z_2 \cdot \left\langle \frac{\sigma_1}{1-D_C} \right\rangle_+ \cdot \varpi \cdot \sinh\left(z_3 \cdot \sqrt{\bar{\rho}} \cdot D_i\right) \cdot \dot{\varepsilon}_p$$

$$\sigma = E(\varepsilon_T - \varepsilon_e)$$

Dc: Damage coalescence

$\sigma_1/(1-D_C)$ maximum principal stress acting on the non-damaged area

$\bar{\rho} = \dfrac{\rho - \rho_0}{\rho_{max} - \rho_0}$ normalised dislocation density

$\dot{\bar{\rho}} = k_1 \cdot \left(1 - \sqrt{\bar{\rho}}\right) \cdot \dot{\varepsilon}_p$ dislocation storage and dynamic recovery

$\dot{\bar{\rho}}_{STATIC} = c_1 \bar{\rho}^{c_2}$ static recovery

$R = B\sqrt{\bar{\rho}}$ isotropic hardening

$k = k_0 \exp\left(\dfrac{Q_p}{\kappa T}\right) \quad c_1 = c_0 \exp\left(\dfrac{-Q_R}{\kappa T}\right)$

Di: Damage at inclusion

ϖ : spatial variation of spacing to diameter ratio

$E = \dfrac{E_0}{\cosh^2(K_1(T - T_0))} \quad B = \dfrac{B_0}{\cosh^2(K_1(T - T_0))}$

Figure 17. Constitutive Viscoplastic model 2 (Foster et al, 2008).

(a) (b)

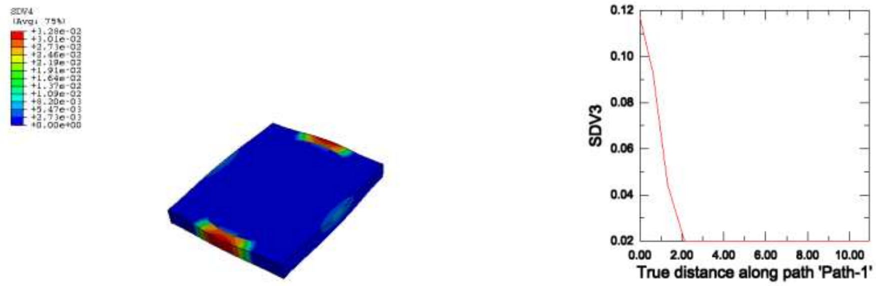

Figure 18. (a) Coalescence state variable SDV4 (b) Path plot of damage growth at inclusion (path 3 of RPS specimen).

4. MicroFEMs

A range of 2D MicroFEM models of inclusions and steel matrix have been developed to assess the influence of biaxial testing with various triaxiality setting (from 0.7 to 1.7), inclusion plasticity, morphology and spacing. The objective is to predict strain increase due to inclusion impingement compared to far field strain (no inclusion interaction). Influence of inclusion hardness v matrix has also been studied. Debonding and crack growth has also been studied by incorporating a Gurson type porosity model (nucleation and growth) within the ABAQUS microFEM at the MnS inclusions to represent low nucleation site for debonding (for instance assuming Pb is precipitating). Strain tends to concentrate around hard inclusion at tip of MnS inclusions with small interaction between different clusters (Figure 19). The closer the inclusions, the greater the strain concentration is developed (up to x3). When inclusions are softer than the matrix (taking into account matrix hardening), more interactions between the various inclusion clusters are developed, i.e. less strain concentration is predicted. The triaxiality has a greater effect when the interspacing of inclusion increases to a given threshold with an inverse predicted behaviour between hard and soft inclusion. As triaxiality increases, strain tends to be less concentrated at soft inclusions which are less closely spaced. For closely spaced inclusions s/d<2, the interdistance between inclusions is the most significant parameter affecting strain concentration, as triaxiality and hardness of inclusion have little effect.

A two-3D inclusion sub-volume microFEM model has also been constructed to assess the influence of straining, hardening and inclusion/matrix interaction (Figure 20). Cases shown represent deformation experienced by surface/subsurface of RPS specimens. Hard inclusion/soft matrix promotes strain concentration between inclusions mostly as inclusion spacing is reduced (same behaviour as in 2D biaxial test). The 3D case shows also the importance of the matrix hardening in reducing strain localisation (Figure 20 (b)). A relation between strain concentration and plasticity index (i.e. ratio between inclusion plasticity and matrix, assuming no recrystallisation (if ratio less than 1, inclusions are less deformable)) has also been derived as shown in Figure 21.

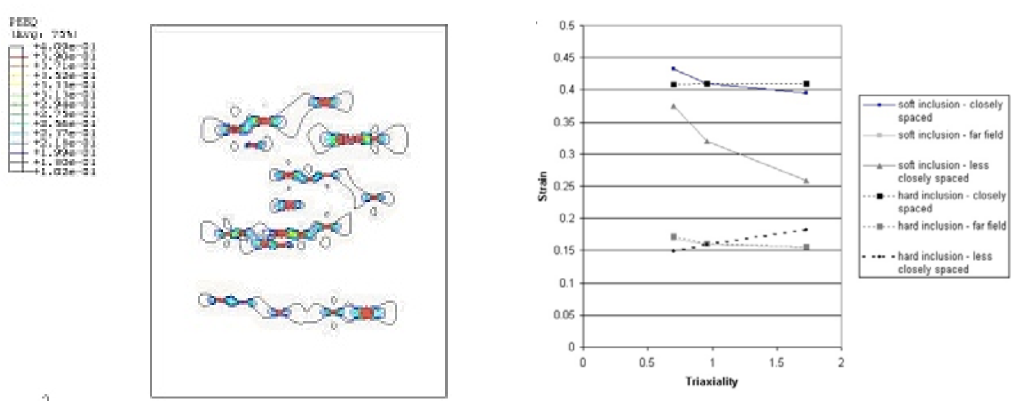

Figure 19. 2D MicroFEM (biaxial test) to study influence of triaxiality, spacing and plasticity of inclusion.

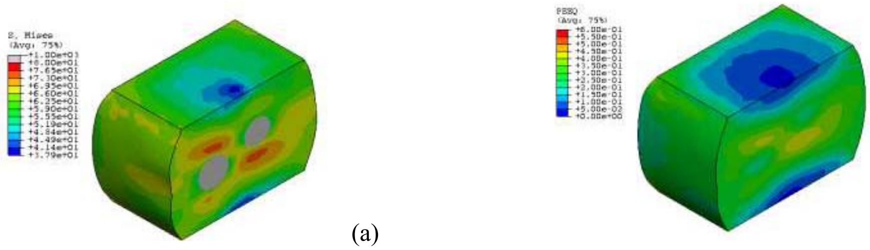

(a) (b)

Figure 20 (a - b). 3D microFEM models (approx. 50 microns^2) (a) 3 directional straining with hard inclusions and soft matrix) (b) 3 directional straining with hard inclusions and hard matrix.

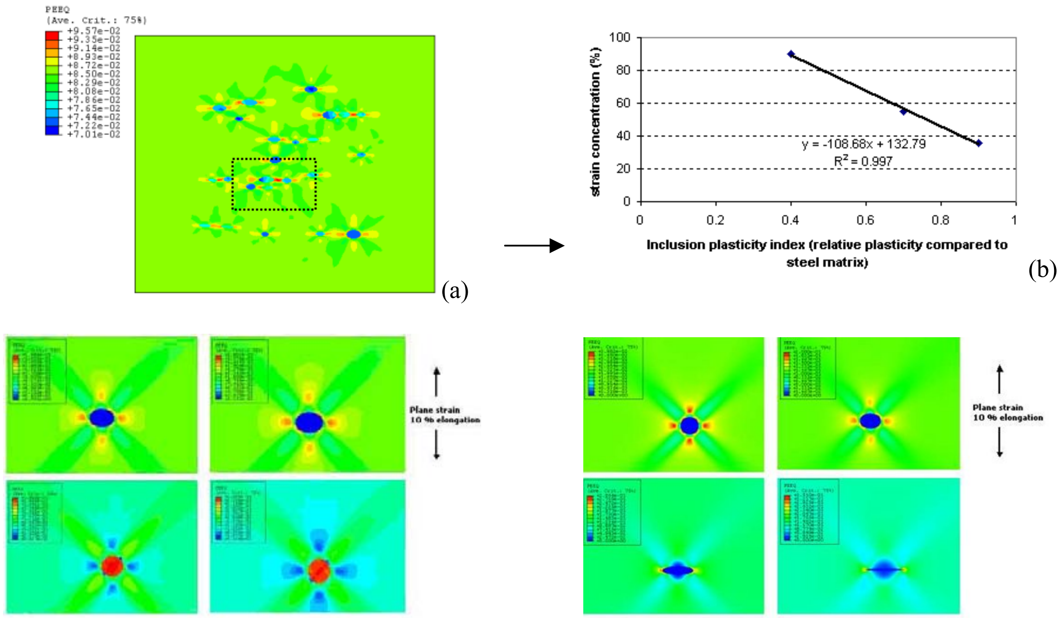

(a) (b)

(c) (d)

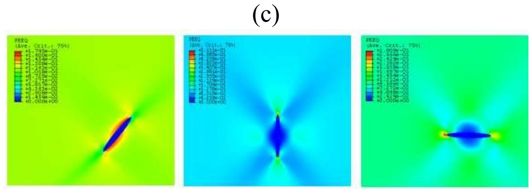

(e)

Figure 21 (a-e). 2D microFEM to study (a,b) effect of inclusion plasticity on strain concentration, (c) effect of hardening of inclusion (d) effect of inclusion shape (e) effect of inclusion orientation to stress field (vertical).

5. CAFE multiscale modelling

The set of ordinary differential equations describing the viscoplastic-damage constitutive Model 1 of Section 3.1 and the CAFE Framework taken from Shterenlikht (2003) from Sheffield University have now been combined into a hybrid multiscale model. The constitutive model is physically-based and capable of modelling both the macro, i.e. stress, strain, material hardening, etc, and microscopic, i.e. average grain size, fraction of recrystallisation, damage, etc, aspects of a material during deformation. The Sheffield CAFE model allows more than 1 CA array, each of which encapsulating a given material law, to be combined and made use of within a Finite Element (FE) simulation. The resulting hybrid of the two cutting-edge modelling capabilities allows the modelling of "*real life*" deformation processes that are traditionally very difficult to deal with and require the consideration of non-uniformity within material microstructure. The sophistication in using the user subroutine in a hybrid mode is that it allows for layers of damage mechanisms to be incorporated seamlessly into the modelling. At present, two categories of damage mechanisms are implemented: (1) ductile damage based on viscoplastic-damage Constitutive Equations of Model 1; and (2) brittle damage based on fraction stress. In this paper the CA modelling of brittle cells is not considered. A CA array is a discrete time entity composed of a finite number of cells. The space of cell states is also discrete. In classical CA formulation, the state of cell m, ψ_m, at time t_{i+1} is completely defined by the state of this and the neighbouring cells at time t_i:

$$\psi_m(t_{i+1}) = \Omega\left(\psi_m(t_i), \psi_l^m(t_i)\right) \tag{12}$$

where $\psi_l^m(t_i)$ is the state of cell l from the neighbourhood of cell m at time t_i; $l = 1,\ldots,L$ and L the number of cells in the neighbourhood of cell m; $m = 1,\ldots,M$ and M the total number of cells in the CA array; and Ω the transition rule.

Contrary to standard CA formulation, in this CA model, the cell size in the ductile CA array is related to the ductile damage cell size. The total number of cells in the ductile CA array M_{D} is chosen such that the linear size of an individual cell is close to the ductile damage cell size L_{D}. Assuming a cubic FE of size $L_{\mathrm{FE}} \times L_{\mathrm{FE}} \times L_{\mathrm{FE}}$, the following equation can be used to choose M_{D}:

$$\frac{L_{\mathrm{FE}}}{\sqrt[3]{M_{\mathrm{D}}}} = L_{\mathrm{D}} \tag{13}$$

When brittle behaviour is considered, a second CA array is used and any loss of material integrity, whether due to ductile or brittle fracture, has to be correctly accounted for in both CA arrays. In this simpler case, the relationship between the CA arrays and FE is done via transfer of solution-dependent state variables at each FE integration point and cell states of the corresponding CA arrays:

$$\boldsymbol{Y_a}(\boldsymbol{t_{i+1}}) = \Xi\left(\boldsymbol{\psi_{m(\mathrm{D})}}(\boldsymbol{t_{i+1}}), \boldsymbol{\psi_{m(\mathrm{B})}}(\boldsymbol{t_{i+1}})\right) \tag{14}$$

where $Y_a(t_{i+1})$ is solution-dependent state variable a at time t_{i+1}, $a = 1,\ldots,A$, A the total number of solution-dependent state variables that obey the above relationship per integration point, and Ξ the CA-to-FE transfer function.

Each ductile cell m can take one of two possible states: $alive$ or $dead$. At time t_0, all cell states are initialised to $alive$: $\psi_{m(\mathrm{D})}(t_0) = alive$

Each ductile cell m carries only one cell property ($N_{\mathrm{D}} = 1$). This is the value of the critical damage, $\Lambda^1_{m(\mathrm{D})} = \beta^{\mathrm{c}}_m$, which decides when cell m becomes $dead$. A random number generator is used to assign β^{c}_m for each cell at time t_0, with a mean value of 0.2 and standard deviation of 0.05.

Each ductile cell m carries only one time-dependent state variable ($Q_{\mathrm{D}} = 1$). This is the value of the effective damage, $\Gamma^1_{m(\mathrm{D})}(t_i) = \beta_m(t_i)$, which is computed by multiplying the damage at the corresponding FE integration point from the viscoplastic model 1(Liu et al, 2005), with a concentration factor expressed in terms of a material constant $\beta_{\mathrm{DSCC}} = 1.0$ and the FE stress state.

The state of each ductile cell m is determined by the following criterion:

$$\psi_{m(\mathrm{D})}(t_{i+1}) = \begin{cases} alive & \text{if } \beta_m(t_i) < \beta^{\mathrm{c}}_m \\ dead & \text{otherwise} \end{cases} \tag{15}$$

If the number of dead cells in any CA array exceeds its maximum allowable value, a ductile void linkage or brittle crack is assumed to have propagated across the whole FE. Hence, the load-bearing capacity of the FE is considered zero and the FE is removed from the FE mesh.

The CAFE model has been applied (ductile regime only) to the RPS with a central network of CA ductile cells located in the region of interest (mid plane) implemented within a VUMAT user-subroutine.

A typical sequence of operations performed at each time increment for each FE and the corresponding ductile array of the CAFE model is shown as follows:

1. FE Level: Update the stress tensor and solution-dependent state variables related to material constitutive equations;
2. CA Level: Update the cell states for the ductile CA array, based on the ductile criterion from Model 1 (Liu et al, 2005);
3. *CA Level: Synchronise the cell states of both CA arrays, such that the brittle cells that occupy the same physical position as those ductile cells that have just been pronounced $dead$ are given a cell state of $deadD$ (not active in this case);*
4. *CA Level: Update the cell states for the brittle CA array, based on the brittle (not active in this case);*
5. CA Level: Synchronise the cell states of both CA array, such that the ductile cells that occupy the same physical position as those brittle cells that have just been pronounced $deadB$ are given a cell state of $dead$; and
6. FE Level: Update solution-dependent state variables $Y_1(t_i)$, $Y_2(t_i)$, and $Y_3(t_i)$. If the $Y_1(t_i)$ for a given FE is equal to $dead$, set the corresponding stress tensor to zero's and remove the FE from the FE mesh.

The model which incorporates the viscoplastic damage equations based on Model 1 (see Figure 15) shows correct behaviour of damage initiation during RPS, but in view of the complexity of the approach and the number of statistical parameters, more work is required to further test the sensitivities of the model to ductile damage (Figure 22).

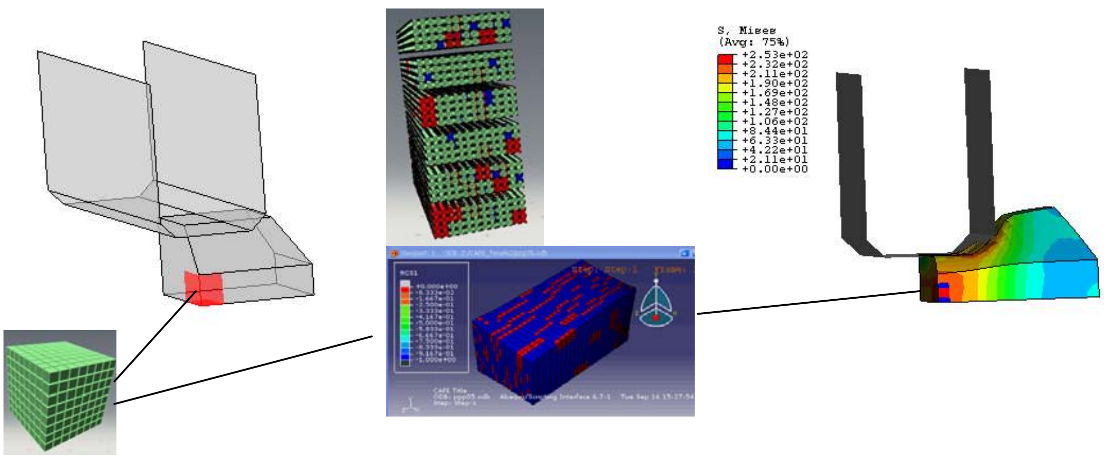

Figure 22. CAFE “coarse” model (CA arrays associated with 270 elements FEM CAFE partition) One-scale transition, (4x4x4) ductile cells array Ld ~2 to 5Nv$^{-1/3}$ ~ 1.8 to 4.4 μm with Nv average number of inclusions per unit volume [in this model - CA ~75μm]- No deformation gradient within CA only for visualization, Viscoplastic damage model 1 (Liu et al, 2005): 25 microns Grain size - 900^{o}C 1s^{-1}.

6. Conclusions and way forward

A 5-step modelling framework using the ABAQUS/Explicit formulation has been developed and presented in this paper, addressing industrial and length scale issues of high temperature damage modelling. This approach (still under development) is based on detailed understanding of nucleation, growth and coalescence as presented in Farrugia, 2008. More work is required at microscale to allow new evolution equations to be derived and incorporated into viscoplastic mesoscopic models with the view to augment simple industrial post-processing damage criteria. The CAFE multiscale modelling requires more development for incorporating the underlying physics and metallurgical phenomena acting at that scale. These developments also pave the way for more detailed studies of effect of inclusion plasticity and decohesion with austenite matrix using more physical polycrystal plasticity models allowing for decohesion (Dunne et al, 2008). These should be supported by advanced microscopic characterisation as that obtained by 3D-Xray tomography. Use of advanced ABAQUS features (sub-modelling, damage, VUMAT, C++ API) are demonstrated with also the need for further developments in ABAQUS to incorporate faster and better ways for post processing results and dealing with damage/crack and fracture modelling.

References

1. Argon, A S, “Mechanics and physics of brittle to ductile transitions in fracture”, Journal of Engineering Materials and Technology 123, pp. 1-11, 2001.
2. Bandstra J. et al., “Modelling void coalescence during ductile fracture of a steel”, Materials Science & Engineering”, A336, pp. 269-281, 2004.
3. Cescotto, S and YY.Zhu, “ Modelling of ductile fracture initiation during bulk forming”, in Complass 95 Owen et al meds, Pineridge Press 1995, pp. 987-997, 1995.
4. Cockroft, M G and Latham, D J, “A simple criterion of fracture for ductile metals”, National Engineering Laboratory, report No240, 1966.
5. Cocks, A C F and Ashby, M F, “On creep fracture by void growth”, Progress in materials science, 27, pp. 189-244, 1982.
6. Dunne et al : http://www.eng.ox.ac.uk/solidmech/publications/FD_Papers/ref12.pdf, 2008
7. Farrugia, D., “Prediction and avoidance of high temperature damage in long product hot rolling”, Journal of Materials Processing Technology Volume 177, issues 1-3 July 2006, pp. 486-492, Proceedings of the 11th International Conference on Metal Forming 2006.
8. Farrugia, D. “Revised plane strain mechanical testing for studying ductile damage of free cutting steel”, vol 2, pp 361-368, Proceedings of the 12th International Conference on Metal Forming 2008, Krakow, 2008.
9. Foster, A D, Lin J, Liu Y, Farrugia, D C J and Dean, T A., “Constitutive modelling of damage accumulation during the hot deformation of free-cutting steels”, Proceedings of the 8th ESAFORM Conference on Material Forming, ESAFORM 2005, 27th-29th April 2005, Romania, Vol. 1, pp. 201-204, 2005.
10. Foster A. D., Lin J., Farrugia D.C.J, Dean T.A., “An Investigation into Damage Nucleation and Growth for a Free-Cutting Steel at Hot Rolling Conditions”, J. of Strain Analysis. Vol 42, 2007, pp. 227-235. ISSN 009-3247. DOI: 10.1243/03093247JSA230, 2007.
11. Foster A.D., Lin J., Farrugia D.C.J., Dean T.A, “Constitutive modelling of damage accumulation during the hot deformation of free-cutting steels, Proceedings of the 8th Esaform Conference on Material Forming”, Volume 1, pp. 201-204, 2005.
12. Foster, A: PhD, 2007, “Modelling of damage evolution under complex strain path and stress-states in hot deformation“, Birmingham University, 2007.
13. Hillerborg, et al, “Analysis of crack formation and crack growth in concrete by means of fracture mechanics and finite elements”, Cement and Concrete Research 1976, vol. 6 pp. 773-782, 1976.
14. Lemaitre J, “How to use damage mechanics”, Nuc.Eng & Des, Vol 80, pp. 233-235, 1984.
15. Lin, J, Liu, Y, Farrugia, D C J and Zhou, M., ”Development of dislocation based-unified material model for simulating microstructure evolution in multipass hot rolling”, Philosophical Magazine A, Vol. 85, No. 18, pp. 1967-1987. ISSN 1478-6435, 2005.
16. Lin, J., A. D. Foster, Y. Liu, Farrugia D.C.J. and T. A. Dean, “On micro-damage in hot metal working Part 2: Constitutive modelling”, J. of Engineering Transactions. 55(1), pp. 1-18. ISSN: 0867-888X, 2007.
17. Liu, Y., Lin, J, Dean, T A and Farrugia, D C J., “A numerical and experimental study of cavitation in a hot tensile axisymmetric testpiece“, Journal of Strain Analysis, 40, pp. 571-586, 2005.
18. Liu Y., Foster A. D., Lin J., Farrugia D.C.J., T. A. Dean, “On micro-damage in hot metal working Part 1: Experimental investigation”, J. of Engineering Transactions. 54(4), pp. 271-287, ISSN 0867-888X, 2006.
19. McClintock, F A., “A criterion for ductile fracture by the growth of holes“, Journal of applied mechanics June 1968, pp. 363-369 Transations of the ASME, 1968.
20. Oyane, M., “Criteria of ductile fracture strain”, Bulletin of JSME, 15, pp1507-1513, 1972.
21. Paliwoda G., Wilson W., Conf on mechanical working on steel, Proc AIME, vol. 21, pp. 126-142, 1963.
22. Rice, J R and Tracey, D M: “On the Ductile Enlargement of voids in triaxial stress Field”, J.Mech.Phys.Solids 17, pp. 201-217, 1969.
23. Shterenlikht, A., “3D CAFE Modeling of Transitional Ductile – Brittle Fracture in Steels”, PhD Thesis, University of Sheffield, Sheffield, 2003.